文章编号: 1001－2060(2006)06－0628－04

管式 SOFC 热电特性的三维数值研究

张兄文, 李　军, 李国君, 丰镇平
(西安交通大学 能源与动力工程学院, 陕西 西安 710049)

摘　要: 建立了固体氧化物燃料电池(SOFC)完整极化的电化学模型与电势方程、$N-S$ 方程耦合求解方法, 对一管式固体氧化物燃料电池的热电特性进行了三维数值模拟, 得到电池发电特性的计算值与实验值吻合良好。分析了电动势分布、电流密度分布、温度分布、电化学反应生成热以及欧姆热分布特性, 计算结果表明电池阴极欧姆极化损失和活化极化损失占全部损失达 85%, 化学反应热约占总生成热的 92%, 欧姆热占 8%。

关　键　词: 管式固体氧化物燃料电池; 数值模拟; 热电特性
中图分类号: M911.42　　文献标识码: A

1　前　言

固体氧化物燃料电池(SOFC)作为一种高效、低排放的先进发电方式, 日益受到了人们的关注。其几何结构主要有板式、管式和单一整体形式。管式 SOFC 具体结构紧凑、能承受较高的工作压力等特点, 目前, 美国西屋公司开发的管式 SOFC 已经有了示范性工程。

SOFC 的平均工作温度一般在 800～1 000℃, 在实验条件有限的情况下, 数值模拟的方法是分析其工作特性的一种有效手段, 可以达到提高其设计水平和降低成本的目的, 并且为建立 SOFC 动态模型提供支持[1]。燃料电池的热动力计算模型是影响数值分析精度的重要因素, 众多学者在这方面做了大量工作[2～6], 但多数局限于采用一维、二维模型模拟, 且模型中对极化损失做了一些简化, 降低了数值模拟的精度, 如文献[5]计算得到的一管式 SOFC 发电特性在低电流密度时与实验误差达到 17%。Chan 发展了一种完整极化计算模型, 提高了计算精度[7], 适用于很宽的电流密度范围, 但该文对模型仅作了定性的分析, 没有得到实验的验证。除文献[3]外, 上述模型均不能反映 SOFC 内部导电区域的电势、电流密度以及欧姆热分布情况。

本文在完善了完整极化损失模型的基础上, 通过 Fluent 提供的 UDF 接口, 将 SOFC 电化学计算模型与电势方程、$N-S$ 方程耦合求解, 对一管式 SOFC 单元的工作特性进行了三维数值模拟, 重点就 SOFC 单元内部热电特性进行了分析。

2　电化学计算模型

本文主要对由西门子－西屋公司开发的一管式 SOFC 进行计算和分析, 电池单元的几何结构参考文献[8], 其结构由空气导流管、导电体和 PEN 组成, PEN 由阳极、电解质、阴极构成, 在阳极, 燃料自下而上流动, 空气通过导流管自上而下进入阴极, 然后沿阴极自下而上流动。本文只考虑燃料为氢气的情况, 则燃料在电极－电解质之间的催化层, 进行如下化学反应:

在阳极: $H_2+O^{2-}\rightarrow H_2O+2e^-$

在阴极: $0.5\,O_2+2e\rightarrow O^{2-}$

总的反应式为: $0.5\,O_2+H_2\rightarrow H_2O$.

阴极释放的 O^{2-} 通过电解质到达阳极, 与阳极的 H_2 结合, 释放出 e^-, e^- 通过连接体并经外电路到达阴极, 并形成电流。

由能量守恒定律和熵守恒定律得到 SOFC 电化学反应的电动势方程:

$$E=-\frac{1}{n_eF}\left[\sum_i(k_ig_i)_p-\sum_i(k_ig_i)_r\right]-\eta_{act}-\eta_{ohm}-\eta_{conc} \tag{1}$$

式中:

$$g_i(T,p_i)=h_i(T)-Ts_i(T,p_i)$$

$$=\int_{T_0}^{T}c_{P_i}(T)\mathrm{d}T-T\int_{T_0}^{T}\frac{c_{P_i}(T)}{T}\mathrm{d}T-RT\ln\frac{P_0}{p_i} \tag{2}$$

收稿日期: 2006－03－31;　修订日期: 2006－07－13
基金项目: 国家高技术研究发展计划基金资助项目(2002AA503020); 西安交通大学博士论文基金资助项目(DFXJTU2005－01)
作者简介: 张兄文(1975－), 男, 安徽安庆人, 西安交通大学博士研究生.

其中: n_e—电化学反应释放的电子数; F—法拉第常数; k—电化学反应组分当量系数; Gibbs 自由能 g—绝对温度 T 和气体压力 p 的函数; 等压比热容 c_p—T 的函数; η—极化损失; 下标 i—气体组元; p、r—生成物和反应物。

极化损失包括活化极化、欧姆极化以及浓度极化损失。活化极化损失由 Butler-Volumer 方程得到:

$$\eta_{act}=\frac{2RT}{n_eF}\sin h^{-1}\left(\frac{i}{2i_0}\right) \tag{3}$$

式中: i、i_0—电流密度和交换电流密度, i_0 是气体组分浓度和温度的函数, 分别由下式给出[9]:

$$\text{阳极: } i_{0a}=\gamma_a\left(\frac{p_{H_2}}{p_{ref}}\right)\left(\frac{p_{H_2O}}{p_{ref}}\right)\exp\left(-\frac{E_a}{RT}\right)$$

$$\text{阴极: } i_{0c}=\gamma_c\left(\frac{p_{O_2}}{p_{ref}}\right)^{0.25}\exp\left(-\frac{E_c}{RT}\right)$$

式中: γ—参考交换电流密度; E—活化能; 下标 a、c—阳极和阴极。

欧姆极化损失是由于电流载体存在着电阻而产生的电压损失, 其模型用 Arrhenius 方程来表示:

$$\sigma=\frac{A_0}{T}\exp\left(-\frac{E_0}{kT}\right) \tag{4}$$

式中: A_0、E_0、k—常数, 与导体的材料相关。电解质欧姆损失为: $\eta_{ohm}=\delta i/\sigma_e$, δ 为电解质厚度。

浓度极化损失是由于反应物和生成物在电极的多孔介质扩散过程中存在着阻力而产生的, 阳极和阴极的浓度极化损失须分别计算, 由下式给出:

$$\eta_{conc,a}=-\frac{RT}{2F}\left[\ln\left(\frac{p_{H_2}}{p^e_{H_2}}\right)-\ln\left(\frac{p_{H_2O}}{p^e_{H_2O}}\right)\right] \tag{5}$$

$$\eta_{conc,c}=-\frac{RT}{4F}\ln\left(\frac{p_{O_2}}{p^e_{O_2}}\right) \tag{6}$$

式中对数项的分子为化学反应当地气体分压, 分母为式(2)化学反应自由能时使用的气体分压。反应气体在多孔介质中扩散由斐克定律和 Knudsen 扩散来描述, 具体计算过程可参考文献[7]。

3　数值方法

气体流动采用层流模型, 求解的控制方程包括 $N-S$ 方程、组分方程和电势方程, 写成通用形式为[10]:

$$\mathrm{div}(\rho v\phi)=\mathrm{div}(\Gamma_\phi \mathrm{grad}\phi)+S_\phi \tag{7}$$

对于电势方程, 对流项等于零, 扩散系数 $\Gamma_\phi=\sigma$, 组分方程的扩散项采用稀释近似 $\Gamma_i=\rho D_{i,m}$, $D_{i,m}$ 为组分 i 的扩散系数。

3.1　源　项

在发生化学反应的催化层, 组分的变化被加到源项中, 组分运输方程的源项为:

$$S_i=M_ik_i|\vec{i}\cdot\vec{n}|/(2F) \tag{8}$$

式中: M_i—组分的摩尔质量, 当组分 i 为反应物时, 组分当量系数 k 为负值, 反之为正值; $\vec{i}$—电流密度向量; $\vec{n}$—电解质表面法矢。能量方程的源项为:

$$S_q=\sigma\mathrm{grad}\,\Phi\mathrm{grad}\,\Phi+Q_{chem}+Q_{rad} \tag{9}$$

式中: Φ—电势; Q_{rad}—辐射换热产生的源项, 采用离散坐标模型[11]; Q_{chem}—化学反应热, 在阳极反应催化层:

$$Q_{chem}=\Delta Q_e|\vec{i}\cdot\vec{n}|/(2F) \tag{10}$$

式中: ΔQ_e—电化学反应热。在多孔介质中, 气体速度的损失被加到动量方程源项中, 由 Darcy 定律求得。

3.2　边界条件

入口燃料摩尔组分为: H_2 89%, H_2O 11%。工作压力 101 kPa, 燃料入口质量流量按燃料利用率的 85%给定, 空气入口质量按空气过余量 6 给定, 出口给定背压, 外壁面假定绝热, 在电极两端给定电势, 中间电解质按固体壁面处理, 通过电解质的电流密度由电化学反应方程求得。导电部件导电率与温度的关系由表 1 给定。

表 1　部件的导电率[6,8]

部　件	导电率 σ
电解质	$3.401\times10^4e^{-10350/T}$
阳极	$1.117\times10^7e^{1392/T}$
阴极	$1.232\times10^4e^{-600/T}$
导电体	$2.918\times10^3e^{-4690/T}$

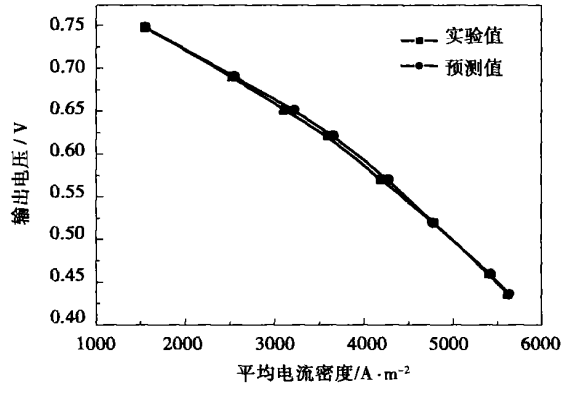

图 1　发电特性的模型预测值与实验值比较[8]

4 结果分析

西门子—西屋公司给出了以阴极支撑结构的管式SOFC 分别在 101 ~ 1515 kPa 工作压力条件下的实验结果[8]，本文计算的SOFC 与实验中采用的SOFC 几何尺寸相同，图 1 给出了101kPa 工作压力、以氢气为燃料的管式SOFC 单元发电特性的计算值与实验值比较图，可以看出计算结果与实验值总体上符合良好，可以验证本文计算模型的可靠性。在平均电流密度 3000 A/m^2 左右，计算值比实验值稍微偏高，主要是极化损失模型精度以及反应气体在多孔介质中传递过程模型的精度有关。

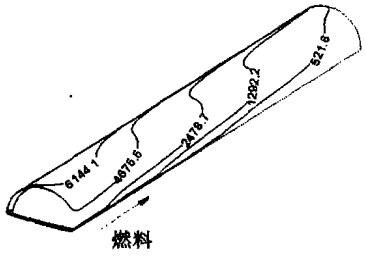

(a) 电解质层电流密度分布(A/m²)

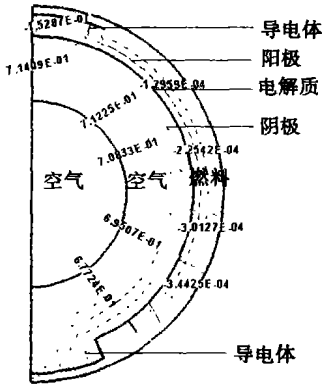

(b) 中截面电流密度向量及电势分布

图 2 电解质层电流密度及中截面电流密度和电势分布

后面的分析都是基于输出电压为 0.652 V，平均电流密度为 3218 A/m^2 情况下的计算结果。图 2(a)为沿气体流动方向流过电解质层的电流密度分布图。由图可得，在初始段区域的流过电解质层的电流密度也大，这是因为开始段反应物的摩尔浓度较高，相应的化学反应更剧烈，相应的化学反应生成电动势也越高。图 2(b)为中截面上电流密度向量和电势分布图。由图看出，电流沿阴极流动过程中的欧姆损失比阳极大得多。

图 3 给出了中截面各种极化损失沿电流流动方向的分布图。横坐标为圆周角，在电流流动方向，取 0°~180°，图中下角 a、e、c 分别表示阳极、电解质和阴极；ohm、act、conc 分别表示欧姆损失、活化极化损失和浓度极化损失。可以看出，阴极的欧姆损失最大，电解质层的欧姆损失和阳极的浓度极化损失较小(阴极浓度极化损失极小，图中没有画出)，而阳极欧姆损失极小，因为其导电率大。本文对各损失进行了统计分析，平均而言，阴极欧姆损失和活化损失之和占全部损失约 85%。

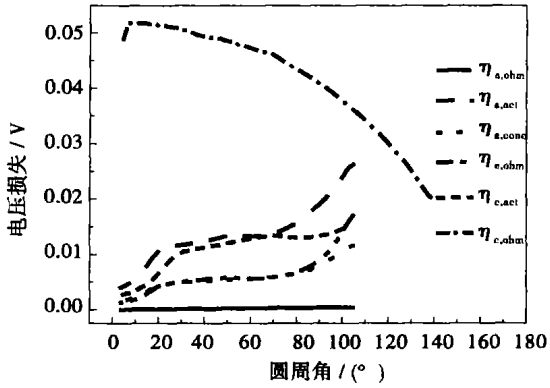

图 3 SOFC 的极化损失($z = L/2$)

图 4(a)为电解质层的温度分布图，由图看出，沿气体流动方向，中部区域温度较高，两端温度较低。因为气体流动过程中不断吸收因电化学反应而放出的热量，但是在端部区域主要受入口较低温度气体冷却的影响。图 4(b)为中截面温度分布图，在半径方向，空气导管中的温度梯度较大。在空气导流管内，受热梯度的影响而产生对流，气体由高温区向低温区流动，在 PEN 两

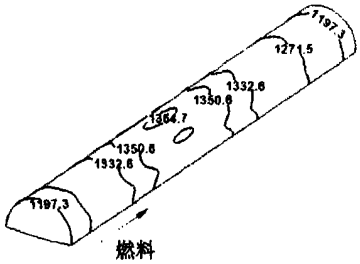

(a) 电解质层温度分度(K)

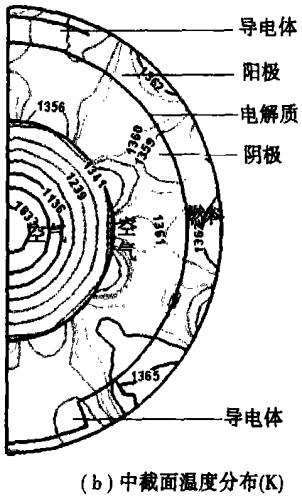

(b) 中截面温度分布(K)

图 4 电解质层及中截面温度分布

侧, 气体流动主要受电解质层两侧电化学反应的推动作用, 在阴极侧, 气体向电解质催化层迁移, 在阳极侧, 气体自电解质阳极催化层向外扩散。

图 5 给出了中截面上电流密度与欧姆热的分布特征, 电流密度是影响欧姆热的主要因素之一。由于阳极厚度比阴极小, 所以其电流密度较大, 在阳极, 沿电流流动方向越来越小, 在阴极, 沿电流流动方向越来越大。阴极的欧姆热比阳极产生的欧姆热大得多, 因为阴极的导电率较低。数值计算结果表明: 在输出电压为 0.652 V, 平均电流密度为 3 218 A/m^2 情况下, 化学反应生成热为 78.1 W, 约占总发热量的 92%, 欧姆热为 6.7 W, 占总发热量的 8%。

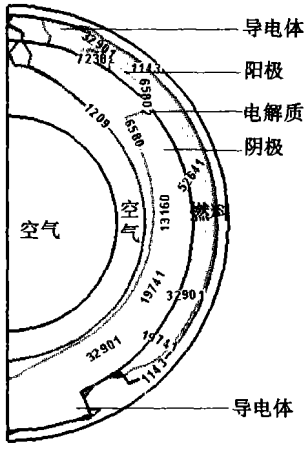

图 5　中截面电流密度及欧姆热分布

5　结　论

采用完整极化的电压损失模型对一管式 SOFC 进行了三维数值模拟, 主要就管式 SOFC 内部热电特性进行了分析, 可以得出以下结论:

(1) 本文建立的完整极化损失模型与电势方程、$N-S$ 方程耦合求解方法具有较好的精度, 能准确的预测 SOFC 的发电特性。

(2) 在一定的工作压力下, 反应物浓度越大, 生成电动势越大, 相应电流密度也大。对于管式 SOFC, 电压损失中的阴极欧姆损失最大; 其次为活化极化损失, 再次是电解质欧姆损失和阳极浓度极化损失。统计表明, 阴极欧姆损失和活化极化损失之和平均占总损失的 85%。

(3) 沿气体流动方向, 温度的最大值在中部。化学反应生成热与流过电解质层电流密度分布相一致, 而欧姆热主要与导电率相关, 阴极产生的欧姆热比阳极大得多。输出电压为 0.652 V, 平均电流密度为 3 218 A/m^2 情况下的计算结果表明, 化学反应生成热占总生成热的 92%, 欧姆热占 8%。

参考文献:

[1] ZHANG XIONG WEN, LI JUN, LI GUO JUN, *et al*. Development of a control-oriented dynamic model for the solid oxide fuel cell [J]. **Journal of Power Sources**, 2006, **160**(1): 258—267.

[2] BRAUN R J. Optimal design and operation of solid oxide fuel cell systems for small-scale stationary applications [D]. USA: University of Wisconsin-Madison, 2002.

[3] FERGUSON J R, FIARD J M, HERBIN R. Three-dimensional numerical simulation for various geometries of solid oxide fuel cells [J]. **Journal of Power Sources**, 1996, **58**: 109—122.

[4] YAKABE H, OGIWARA T, HISHINUMA M, *et al*. 3-D model calculation for planar SOFC [J]. **Journal of Power Sources**, 2001, **102**: 144—154.

[5] LI P W, SUZUKI K. Numerical modeling and performance study of a tubular SOFC [J]. **J Electrochem Soc**, 2004, **151**(4): A548—A557.

[6] BESSETTE N F, WEPFER W J, WINNICK J. A mathematical model of a solid oxide fuel cell[J]. **J Electrochem Soc**, 1995, **142**: 3792—3800.

[7] CHAN S H, KHOR K A, XIA Z T. A complete polarization model of a solid oxide fuel cell and its sensitivity to the change of cell component thickness [J]. **Journal of Power Sources**, 2001, **93**: 130—140.

[8] WILLIAMS M C. Fuel cell handbook 6th ed[M]. USA West Virginia: EG & G Technical Services Inc Science Applications International Corporation, U S Department of Energy Office of Fossil Energy, National Energy Technology Laboratory, 2002.

[9] COSTAMAGNA P, HONEGGER K. Modeling of solid oxide heat exchanger integrated stacks and simulation at high fuel utilization [J]. **J Electrochem Soc**, 1998, **145**(11): 3995—4007.

[10] 陶文铨. 数值传热学[M]. 第二版. 西安: 西安交通大学出版社, 2001.

[11] Fluent Inc. Fluent User's Guide Version 6.1[M]. USA New Hampshive: Fluent Inc, 2003.

(何静芳　编辑)

mentioned combustion can be accompanied by a dispersion combustion reaction in the furnace as a whole. As the combustion gases can be blended in the furnace uniformly and the combustion reaction is stable, a low quantity of CO is produced. An experimental study as well as calculations and analyses indicate that CO is mainly generated in a cylindrical space of φ400 mm about 600 mm ~3000 mm away from the burner spray nozzle. In other areas outside the cylindrical space, the combustion proceeds fully and almost no CO is produced. Excess air factor and volumetric heat release rate have little effect on the generation quantity of CO in flue gases. Compared with traditional flame combustion and present-day high-temperature air flameless combustion, the flameless combustion of normal-temperature air features a low CO generation quantity and stable emissions. **Key words**: flameless combustion of normal-temperature air, CO generation, experimental study

TGA 基点漂移量的测试与分析=**Measuring-testing and Analysis of TGA Base-point Drift Magnitude**[刊, 汉] / YU Na, FU Pei-fang, ZHOU Huai-chun (National Key Laboratory on Coal Combustion under the Central China University of Science and Technology, Wuhan, China, Post Code: 430074) // Journal of Engineering for Thermal Energy & Power. — 2006, 21(6). —618 ~622

The base-point drift magnitude pertains to the same order of magnitude as the low-temperature oxygen absorption quantity of coal and can seriously affect the accuracy of experimental results. It has been found during experiments that the base-point drift magnitude of a high-precision STA 409C thermogravimetric analyzer could reach 3% to 7% with its absolute value being 0.2 to 0.5 mg. Through a theoretical calculation and the use of TGA blank experiment method, the main factors affecting STA 409C base-point drift magnitude are identified as the temperature-rise caused buoyancy increment assuming the same direction as gravity, the lifting forces of streaming and a viscid tractive force sparked by an upward gas flow. To choose an appropriate gas flow rate, slow down the speed of temperature rise, change the constituent of gases inside the furnace to decrease density and enhance the emission and absorption capacity of gases can all contribute to decreasing the base-point drift magnitude. When the base-point drift magnitude reaches 7%, the deviation of activation energy will be 0.28%. **Key words**: TGA (thermogravimetric analyzer), base-point drift, variation in buoyancy, variation in lifting forces

对用烃类和氨为还原剂的脱硝技术的计算分析=**Calculation and Analysis of Denitration Technology with Hydrocarbons and Ammonia Serving as a Reducing Agent**[刊, 汉] /ZHANG Yan-wen, CAI Ning-sheng (Education Ministry Key Laboratory on Thermal Sciences and Power Engineering under the Tsinghua University, Beijing, China, Post Code: 100084) // Journal of Engineering for Thermal Energy & Power. — 2006, 21(6). —623 ~627

Through the adoption of a plug flow reactor in Chemkin 4.0 software package and chemical dynamic models established by Miller (1989) and others, a simulation calculation and contrast analysis have been conducted of the principle of reburning, advanced reburning, SNCR (selective non-catalytic reduction) and hydrocarbon-added SNCR reactions. In this connection, the effect of different reaction temperatures, reburning fuel ratios and residence time on denitration efficiency has also been studied. The calculation results show that the advanced reburning with the introduction of an amido reducing agent is better than conventional reburning technology, because it can broaden the effective temperature range for the denitration process, accelerate the reaction speed and enhance denitration efficiency by about 20%. The addition of a very small quantity of hydrocarbon (hydrocarbon/NO< 1) in the SNCR reaction can widen the effective denitration temperature range, speed up the denitration reaction rate, shorten the time required for completing the denitration reaction by one half and attain a comparatively high denitration efficiency at a relatively low reaction temperature. However, the advanced reburning will need over and above more than 15% of reburning fuel to reach a corresponding denitration efficiency. **Key words**: nitrogen oxide, reduction, denitration, reburning, advanced reburning, selective non-catalytic reduction

管式SOFC 热电特性的三维数值研究=**A Three-dimensional Numerical Study of Thermoelectric Characteristics of Tubular Solid-oxide Fuel Cells**[刊, 汉] /ZHANG Xiong-wen, LI Jun, LI Guo-jun, et al (College of Energy Source

and Power Engineering under the Xi' an Jiaotong University, Xi' an, China, Post Code: 710049) // Journal of Engineering for Thermal Energy & Power. — 2006, 21(6). — 628 ~ 631

A method has been established for solving a full polarization electrochemical model for solid oxide fuel cells (SOFC) coupled with a potential equation and N-S one. A three-dimensional numerical simulation was conducted for the thermoelectric characteristics of the tubular SOFC. The calculated values of power generation characteristics of the cells obtained are in good agreement with the experimental ones. Meanwhile, the electric motive force distribution, electric current density and temperature distribution, electrochemical reaction-produced heat and Ohm heat distribution characteristics were also analyzed. The calculation results show that cathode Ohm polarization and activation polarization losses of the cells would account for 85% of the total losses, while chemical reaction-produced heat would account for about 92% and Ohm heat for 8% of the total heat generated. **Key words**: tubular solid oxide fuel cell, numerical simulation, thermoelectric characteristics

旋转型气-液雾化喷嘴的雾化特性研究=**A Study of Atomization Characteristics of "Swirling Gas-liquid Spray Atomizers"** [刊, 汉] /GONG Jing-song, FU Wei-biao (Engineering Mechanics Department, Tsinghua University, Beijing, China, Post Code: 100084) // Journal of Engineering for Thermal Energy & Power. — 2006, 21(6). — 632 ~ 634, 639

By using a laser-phase Doppler analyzer (PDA), an experimental study was conducted of the atomization characteristics of "Swirling Gas-liquid Spray Atomizers". Water was used as the liquid to be atomized instead of oil and compressed air employed as an atomization medium. The parameters of atomization characteristics under different operating conditions were measured, such as Sotyl mean diameter and particle speed of atomized droplet particles etc. The experimental measurement results indicate that the atomizer can achieve a comparatively good atomization state under the condition of a relatively small gas-liquid ratio with the average SMD of droplets at the center reaching 40 μm. With an increase in pressure and gas-liquid ratio, the atomization level will be enhanced accordingly. However, it is scarcely affected by the structure of the atomizer. The research findings can provide an underlying basis for the practical design of atomizers. **Key words**: "Swirling Gas-liquid Spray Atomizers", PDA (Phase Doppler Analyzer), atomization characteristics

迷宫密封转子动特性三维CFD数值的研究=**A Study of Methods Used for Three-dimensional CFD (Computational Fluid Dynamics) Numerical Analysis of Dynamic Characteristics of Rotors with Labyrinth Seals** [刊, 汉] / LIU Xiao-feng, LU Song-yuan (Vibration Control and Information System Research Institute under the Southeast University, Nanjing, China, Post Code: 210096) // Journal of Engineering for Thermal Energy & Power. — 2006, 21(6). — 635 ~ 639

The aerodynamic force produced by fluid in labyrinth seals is a major factor that may lead to instability of a shaft system. This aerodynamic force can be described by a factor of seal dynamic characteristics. A vortex rotor-labyrinth seal three dimensional CFD (computational fluid dynamics) mathematical model was established. With a labyrinth seal at the inlet of a compressor serving as a specific case, the aerodynamic force at the rotor surface was calculated by using a general-purpose CFD software Fluent followed by a calculation of the seal dynamic characteristics factor. The calculated results when compared with those obtained by using another CFD software TASCflow and integrated-flow labyrinth seal calculation program DYNLAB indicate that the accuracy of loss-of-stability calculation under the three-dimensional CFD method is higher than that obtained by using the integrated-flow method. Finally, the impact of such factors as pre-swirling speed at the seal inlet, variation in clearances and cone-shaped axial clearance of seals etc. on seal stability was also calculated and analyzed in detail, thus providing a theoretical basis for decreasing steam flow excitations in seals. **Key words**: labyrinth seal, computational fluid dynamics, steam flow excitation, rotor dynamic characteristics factor

低质量流速垂直管屏技术的原理与应用分析=**Analysis of Working Principle and Application of Low Mass Flow-speed Vertical Tube-platen Technology** [刊, 汉] / LI Yan, ZHAO Xin-mu, YUE Guang-xi, et al (Thermal Energy